Fine-Tuning of Magnetic Anisotropy in Tetranuclear M2Dy2 Complexes with Zig-Zag Topology: The Impact of 3d Metal Selection

Guan-Lin Lu, Shih-Ting Chiu, Jérôme Long, Po-Heng Lin

Fine-Tuning of Magnetic Anisotropy in Tetranuclear M_2Dy_2 Complexes with Zig-Zag Topology: The Impact of 3d Metal Selection

Guan-Lin Lu,[a] Shih-Ting Chiu,[a] Jérôme Long*[b,c] and Po-Heng Lin*[a]

a. Department of Chemistry, National Chung Hsing University, Taichung 402, Taiwan.

b. ICGM, Univ. Montpellier, CNRS, ENSCM, Montpellier, France.

c. Institut Universitaire de France (IUF), 1 rue Descartes, 75231 Paris Cedex 05, France.

Abstract

This study presents the design, synthesis, and magnetic characterization of two novel heterometallic tetranuclear complexes, $[M_2Dy_2(Hheb)_2(heb)_4]\cdot 4MeOH$ (H_2heb = (E)-N'-(1-(2-hydroxyphenyl)ethylidene)benzohydrazide; M = Ni (**1**), Cu(**2**)). These complexes exhibit a rare zig-zag core topology induced by the rigid $Hheb/heb^{2-}$ ligands. A subtle interplay between the incorporated 3d metal ions (Ni^{2+} and Cu^{2+}) and the magnetic properties is evidenced. Notably, the choice of the 3d metal plays a crucial role in modulating the Dy^{3+} ion's coordination environment and axiality, as supported by theoretical calculations. While both complexes exhibit rapid Quantum Tunneling of Magnetization (QTM), complex **1** (Ni^{2+}) demonstrates markedly enhanced slow relaxation dynamics compared to complex **2**. This difference is attributed to the stronger axiality indirectly induced by Ni^{2+} in complex **1**, whereas the Cu^{2+}-induced distortions and ferromagnetic interactions in complex **2** negatively affect the slow relaxation behavior.

Introduction

The development of novel single-molecule magnets (SMMs) with improved magnetic properties continues to be a central theme in materials science.[1-6] These fascinating molecular entities exhibit persistent magnetization even in the absence of an external magnetic field, a property that stems from the unique electronic structure of certain lanthanide ions, particularly Dy^{3+}.[7-19] The magnetic behavior of Dy^{3+} ion is highly sensitive to its coordination environment, and the ability to engineer axial Crystal-Field (CF) makes it a versatile and essential building-block for SMM design.

To enhance SMM properties, incorporating Dy^{3+} ions into polynuclear complexes has emerged has a strategic approach. Ligands with multiple binding sites, such as those featuring phenoxide groups, facilitate magnetic exchange interactions between metal centers. While single-ion anisotropy plays a dominant role in polynuclear SMMs, intramolecular magnetic interactions between the metal centers or metal-radical systems can significantly influence overall magnetic relaxation dynamics, impacting key parameters such as blocking temperature and magnetic coercivity.[20, 21] Understanding these intramolecular magnetic interactions is essential as they can influence relaxation in two ways: (i) by inducing mixing of magnetic states, which can accelerate the Quantum Tunneling of Magnetization (QTM),[22] and (ii) by providing positive effects such as exchange bias, which can alter QTM relaxation and enhance coercivity.[23-27] Recent studies on dilanthanide complexes with strong metal-metal bonding have demonstrated remarkable coercive fields exceeding several Teslas, highlighting the potential benefits of such interactions.[28-30]

Another approach consists in the development of 3d-4f heterometallic complexes, where the combination of 3d and 4f transition metals presents exciting possibilities for introducing significant magnetic interactions or quench the QTM as well as introducing additional functionalities.[31-35] Specifically, Cu/Dy systems often exhibit ferromagnetic interactions, which are generally detrimental to SMM behavior.[33] However, they present an intriguing opportunity: these systems can be used to engineer polynuclear complexes featuring both Dy-Dy and Cu-Dy magnetic interactions, aiming to harness the benefits of both exchange interactions for SMM design.

In parallel, spin-state control, achieved by modulating the coordination environment of metal centers,[36-38] has recently emerged as a useful strategy to fine-tune magnetic interactions and

SMM behavior.[39] While dinuclear 4f-4f[20, 26, 40-50] and 3d-4f[33, 51-54] complexes have been extensively studied, introducing two distinct magnetic exchange interactions necessitates the design of higher nuclearity systems. Although higher nuclearity complexes offer greater structural diversity, achieving precise control over metal ion arrangement and coordination environments remains a significant challenge.

In this context, we report the synthesis, crystals structures, magnetic properties and theoretical calculations of two novel tetranuclear complexes [M_2Dy_2] complexes (M = Ni (**1**), Cu (**2**)). These complexes feature a scarce zig-zag core topology driven by the rigid $Hheb^-$/heb^{2-} ligand. The core comprises two bridged Dy^{3+} ions connected by two peripheral 3d metal ions (Ni^{2+} or Cu^{2+}). This architecture provides a unique platform to elucidate the influence of the 3d metal ion on the Dy^{3+} magnetic environment and its impact on overall magnetic behavior. By comparing the behavior of the complex containing the diamagnetic Ni^{2+} ion (complex **1**) with that of the complex containing the paramagnetic Cu^{2+} ion (complex **2**), we aim to decipher the specific role of 3d-4f magnetic interactions in modulating the SMM properties of these tetranuclear complexes.

Experimental Section

General Conditions

All chemicals and solvents were purchased from Alfa Aesar, and used as received without further purification. ^1H spectra were recorded on a Varian Mercury-400 (400 MHz for ^1H) spectrometer. Infrared spectra were recorded on all samples in the solid-state under ambient conditions on a Nicolet iS5 FT-IR spectrometer with iD5 ATR accessory in the 4000-400 cm^{-1} region.

Synthesis of H_2heb

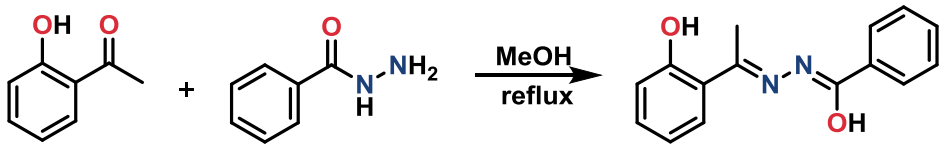

Scheme 1. Synthesis of the H_2heb ligand.

The (E)-N'-(1-(2-hydroxyphenyl)ethylidene)benzohydrazide (H_2heb) were prepared by reacting equimolar amounts of 2'-hydroxyacetophenone and the benzohydrazide, in the methanol at reflux temperature, in accordance with literature procedures.[55]

Synthesis of $[Ni_2Dy_2(Hheb)_2(heb)_4]\cdot 4$ MeOH (1·4MeOH)

To a solution of $Dy(NO_3)_3\cdot 5H_2O$ (0.0625 mmol, 0.0274 g) in MeOH (12.5 mL), a solution of **H_2heb** (0.125 mmol, 0.0318 g) and triethylamine (1 mmol, 0.139 mL) in acetone (5 mL) was added. Subsequently, a solution of $Ni(NO_3)_2\cdot 6H_2O$ (0.0625 mmol, 0.0182 g) in methanol (12.5 mL) was introduced dropwise to the Dy metal solution. The reaction mixture was stirred for 1 min and then filtered. The orange solution was settled and after 5 days, transparent orange crystals of **1** were collected by filtration, washed with ether, and dried *in vacuo*.

Complex **1** : Yield = 45 %. IR (ATR cm^{-1}): 1627 (s), 1594 (m), 1577 (m), 1520 (w), 1478 (m), 1437 (w), 1366 (m), 1317 (m), 1293 (m), 1241 (w), 1021 (s), 845 (s), 745 (m), 702 (w), 688 (m). Anal. (%) calcd. for $C_{90}H_{82}N_{12}Dy_2Ni_2O_{16}$ (2030.07, **$1\cdot 4H_2O$**): C, 53.25; H, 4.07; N, 8.28. Found: C, 53.08; H, 3.71; N, 8.15. CCDC number: 2358670.

Synthesis of $[Cu_2Dy_2(Hheb)_2(heb)_4]\cdot 4$ MeOH (2·4MeOH)

To a solution of $DyCl_3\cdot 6H_2O$ (0.0625 mmol, 0.0235 g) in MeOH (7.5 mL), a solution of **H_2heb** (0.125 mmol, 0.0318 g) and triethylamine (1 mmol, 0.139 mL) in MeOH (15 mL)

was added. Subsequently, a solution of $CuCl_2 \cdot 2H_2O$ (0.0625 mmol, 0.0107 g) in MeOH (7.5 mL) was introduced dropwise to the Dy metal solution. The reaction mixture was stirred for 1 min and then filtered. The green solution was settled and after 5 days, transparent green crystals of **2** were collected by filtration, washed with ether, and dried *in vacuo*. Complex **2**: Yield = 60%. IR (ATR cm^{-1}): 1627 (s), 1589 (m), 1574 (m), 1538 (m), 1515 (w), 1505 (m), 1494 (m), 1478 (w), 1435 (w), 1366 (m), 1293 (m), 1240 (w), 1025 (s), 846 (m), 746 (w), 703 (w), 581 (s). Anal. (%) calcd. for $C_{90}H_{80}N_{12}Dy_2Cu_2O_{15}$ (2021.77, **2·3H$_2$O**): C, 53.47; H, 3.99; N, 8.31. Found: C, 53.71; H, 3.68; N, 8.12. CCDC number: 2358671.

X-ray crystallography

Single crystals of complexes **1-2** suitable for X-ray diffraction measurements were mounted on an Oxford Xcalibur Sapphire-3 CCD Gemini diffractometer employing graphite-monochromated Mo-Kα radiation (λ = 0.71073 Å), and intensity data were collected with ω scans. The data collection and reduction were performed with the CrysAlisPro software, and the absorptions were corrected by the SCALE3 ABSPACK multiscan method. The space-group determination was based on a check of the Laue symmetry and systematic absences, and it was confirmed using the structure solution. The structure was solved and refined with the *Olex2 1.2-ac21* package. Anisotropic thermal parameters were used for all non-H atoms, and fixed isotropic parameters were used for H atoms.

Magnetic Measurements

Magnetic susceptibility data were collected with a Quantum Design MPMS3 SQUID magnetometer working in the range 1.8–300 K with the magnetic field up to 7 Tesla. The samples were filtered and prepared immediately prior to the magnetic measurements in order to minimize any potential degradation. The data were corrected from the sample holder and the

diamagnetic contributions calculated from the Pascal's constants. The AC magnetic susceptibility measurements were carried out in the presence of a 2.5 Oe oscillating field in zero or applied external DC field.

Theoretical Calculations

CASSCF calculations were performed with ORCA 5.0[56, 57] software using the crystallographic structures without any structural geometry optimization. The fragments were generated by substituting a dysprosium ion in the tetranuclear complex by a diamagnetic yttrium ion and the copper ion by diamagnetic zinc ions. Tolerance for energy convergence is fixed at 10^{-7} E_h. An active space considering the seven 4f orbitals with 9 electrons CAS (9, 7) for all the sextets (21 roots) for spin-orbit coupling using QDPT was considered. The def2 Ahlrichs basis sets were used: DKH-DEF2-TZVP for all atoms, except for Dy for which SARC2-DKH-QZVP basis set was employed. The AUTOAUX feature was used to automatically generate auxiliary basis sets within the RIJCOSX approximation to speed up the calculations. Subsequently, the SINGLE_ANISO[58] program implemented in ORCA was utilized to obtain detailed information about magnetic relaxation.

Results and discussion

Synthesis and crystal structures. The $Hheb^{-}$/heb^{2-} derivatives featuring multi-coordination pockets and a rigid scaffold, are ideal for designing polynuclear complexes. Their mixed O/N donor sets facilitate coordination of both 3d and 4f ions.

The heteronuclear [M_2Dy_2] complexes **1** and **2** were prepared through a stepwise process. Initially, a methanolic solution of Dy^{3+} (nitrate for **1** and chloride for **2)** was reacted with a mixture of H_2heb (2 equiv.) and an excess of triethylamine (16 equiv.). Subsequently, the

corresponding M^{2+} salt solution was added (Scheme 2). Crystallization of the resulting solution yielded the heterotetranuclear complexes. Whilst the counter-ions are not incorporated in the complexes, the reaction appears to be anion-dependent. Notably, no crystals of **1** and **2** were obtained using the precursor pairs $DyCl_3/NiCl_2$ or $Dy(NO_3)_3/Cu(NO_3)_2$.

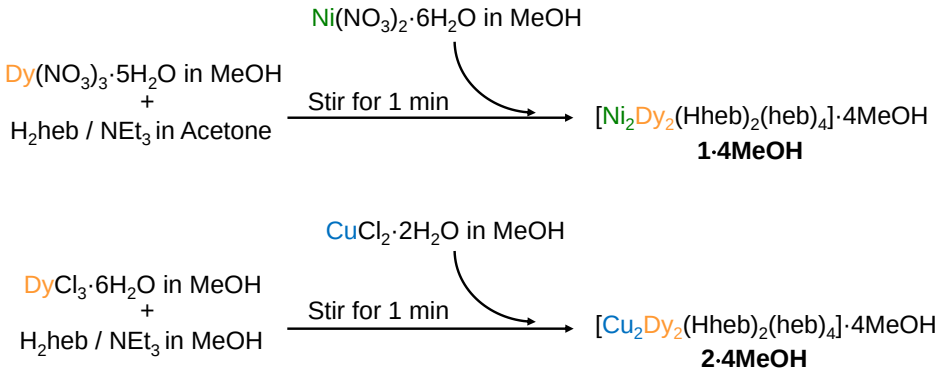

Scheme 2. Synthesis of complexes **1** and **2**.

X-ray analysis reveals that complexes **1** and **2** both crystallize in the triclinic $P\bar{1}$ space group with half a complex in the asymmetric unit (Table S1). This unit contains one Dy^{3+} ion, an associated transition metal ion (Ni^{2+} and Cu^{2+} for **1** and **2**, respectively) and three $Hheb^{-}/heb^{2-}$ ligands. Both complexes **1** and **2** share a similar core, described as centrosymmetric tetranuclear complexes. This core can be further broken down into two heterometallic dinuclear MDy units associated through a central homometallic dinuclear Dy_2O_2 unit, forming a zig-zag arrangement (Figure 1). This core topology is rare, with only a few analogous examples reported in the literature.[59-61] Electroneutrality considerations imply the coexistence of both $Hheb^{-}$ and heb^{2-} ligand forms in the tetranuclear complexes, resulting in the formula $[M_2Dy_2(Hheb)_2(heb)_4]\cdot 4MeOH$ (M = Ni (**1**), Cu(**2**)).

In both complexes, the Dy^{3+} ions are bridged by two phenoxide, with Dy-O bond lengths of 2.344 and 2.353 Å in **1**, and slightly shorter and more asymmetric distances (2.319 and 2.345 Å)

in **2** (Table 1). The Dy-O-Dy angles are wider in **1** (112.48°) compared to **2** (110.56°). In addition, the Dy^{3+} ions complete their coordination sphere with two O and N atoms along with two bridging oxygens that connect to the M^{2+} metal ion, giving an octacoordinated geometry. The Dy-O(-M^{2+}) distances are shorter than those within the homometallic Dy_2 core with values of 2.309(4)/2.449(4) Å and 2.295(5)/2.438(5) Å for **1** and **2**, respectively. The bridging angle values are also consistently shorter (Table 1), with significant asymmetry noticeable for **2**, for which the angles are 103.276°/107.636° and 101.404°/105.9°. The localization of the different ligand moieties can be tentatively determined through an analysis of crystallographic distances. The monoprotonated $Hheb^{-}$ ligand adopts a keto-form, which is expected to exhibit shorter C–O bond lengths with respect to the doubly deprotonated heb^{2-} moieties due to the presence of the ketone group (C=O). For example, in complex **1**, particularly short C–O distances of 1.257(6) Å are observed for the central ligands bridging the two Dy^{3+} ions. This distance can be compared to the longer distances of 1.298(6) and 1.303(6) Å for the peripheral ligands (Table S2). Therefore, the two central ligands connecting the Dy^{3+} ions can be assigned to $Hheb^{-}$, whereas the four peripheral ligands are attributed to doubly deprotonated heb^{2-} moieties, as shown on Figure 1.

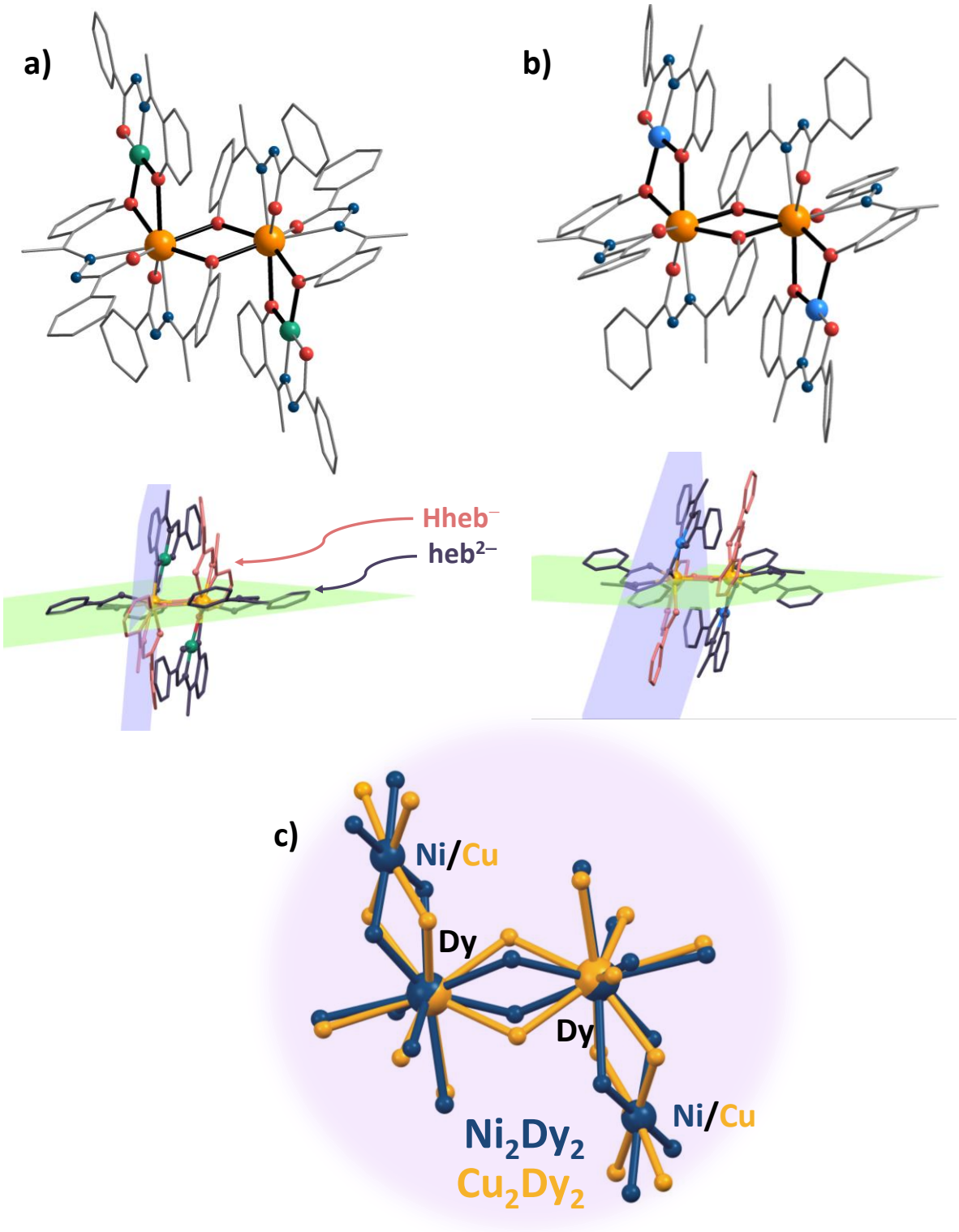

Figure 1 Molecular structures of the complexes **1** (a) and **2** (b). The bottom pictures represent the dihedral planes between the Dy_2 (green plane) and the MDy (purple plane) units and

emphasize the differences in the ligand protonation state based on the crystallographic distances. Colour code: orange, Dy; green, Ni; light blue Cu, N, dark blue; red, O; grey, C. Hydrogen atoms have been omitted for clarity. c) Overlay of the core structure for **1** (blue) and **2** (orange).

Table 1: Selected bond distances and angles.

Compound	Dy−O(-Dy) bridging distances (Å)	Dy-O-Dy bridging angle (°)	Dy−Dy distances (Å)	Dy−O-M distances (Å)	Dy−O-M briding angle (°)	Dy-M distance (Å)	Dihedral angle
1	2.344(4)/ 2.353(3)	112.48(14)	3.905	2.309(4)/ 2.449(4)	103.276/ 107.636	3.390	79.425(116)
2	2.319(5)-2.345(5)	110.56(18)	3.834	2.295(5)/ 2.438(5)	101.404/ 105.9(2)	3.382	80.780(143)

Both M^{2+} ions in **1** and **2** exhibit a square planar coordination environment defined by three oxygen and one nitrogen donor atoms. The geometry of both Dy^{3+} and M^{2+} ions was quantitatively analyzed using the SHAPE software,[62] revealing substantial differences between the two complexes. While the Dy^{3+} ion adopts a distorted square antiprism geometry in both cases, the degree of distortion is slightly higher in **1** (Table S3). Conversely, the square planar geometry of the M^{2+} ion appears more distorted in **2** compared to **1** (Table S4). The intramolecular Dy^{3+} -Dy^{3+} and Dy^{3+} -M^{2+} distances are slightly shorter in **2** (Table 1). The unique structure is further evidenced by the pronounced dihedral angles of approximately 80° observed between the planes of the homometallic Dy_2 and heterometallic MDy units (Figure 1).

For both compounds, hydrogen bonding interactions are observed between methanol solvates and heb^{2-} ligands. The shortest intermolecular Dy^{3+}-Dy^{3+} distances found in the crystals are equal to 11.9870(16) Å and 11.1727(8) Å (Figure S1).

Magnetic properties.

The magnetic properties of the two complexes were investigated using SQUID magnetometry under both static and oscillating fields.

At room temperature, the χT value for **1** of 29.98 $cm^3.K.mol^{-1}$ is slightly higher than the value of 28.34 $cm^3.K.mol^{-1}$ expected for two non-interacting Dy^{3+} ions, considering that the square planar Ni^{2+} ions are diamagnetic. As the temperature decreases, χT progressively decreases to reach a minimum of 23.30 $cm^3.K.mol^{-1}$ at 1.8 K (Figure 2). This behavior likely originates from the thermal depopulation of the Dy^{3+} Kramers doublets (KD), potentially accompanied by weak antiferromagnetic interactions between the Dy^{3+} ions.

The room χT temperature value for **2** of 30.87 $cm^3.K.mol^{-1}$ is in good accordance with the expected value of 29.19 $cm^3.K.mol^{-1}$ for two Dy^{3+} ions and two Cu^{2+} ($S = 1/2$, $g = 2.1$) without magnetic interactions. In contrast to **1**, the thermal dependence of χT exhibits a significant increase below 10 K, reaching a maximum around 3 K, before decreasing at lower temperatures (Figure 2). This behavior strongly suggests the presence of ferromagnetic interactions between the Dy^{3+} and Cu^{2+} ions. Given the similar core structures of **1** and **2**, the occurrence of Dy^{3+} - Dy^{3+} ferromagnetic interactions is unlikely, as evidenced by the absence of a χT increase in **1**.

The field dependence of the magnetization at 1.8 K, reveals typical unsaturated curves for both compounds, indicative of moderate magnetic anisotropy, with values of 11.69 and 13.79 $N\beta$ for **1** and **2** respectively, under a 70 kOe field (Figure 2, inset). The observed difference of 2.10 $N\beta$ in magnetization values is close to the theoretical value of 2 $N\beta$ expected from the contribution of two additional Cu^{2+} ions ($S = 1/2$) in complex **2**.

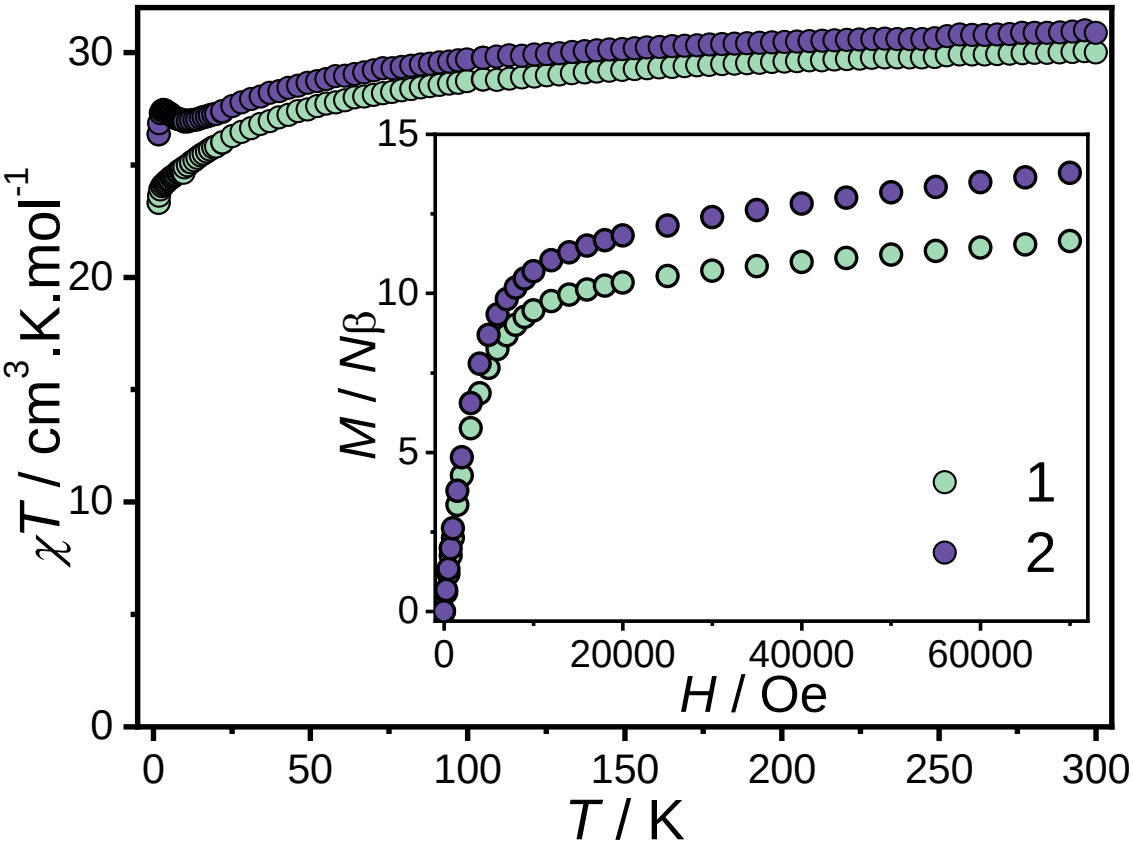

Figure 2. Temperature dependence of χT under an applied magnetic field of 1000 Oe for **1** and **2.** Inset: field dependence of the magnetization at 1.8 K.

Alternating currents (ac) measurements were employed to investigate the occurrence of a slow relaxation of the magnetization. Under zero applied DC field, a weak out-of-phase susceptibility component (χ'') was observed for complex **1**, although it lacked a distinct maximum, indicating the presence of fast QTM. In contrast, no significant χ'' component was detected for complex **2** under the same conditions (Figure S2), suggesting a faster QTM.

To potentially suppress the QTM, ac susceptibility measurements were conducted in the presence of dc fields. Whereas a slight increase in the χ'' component can be observed for **1** at high frequencies up to 1500 Oe, complex **2** exhibits only a weak emergence of χ'' at low frequencies with a maximum signal at 2000 Oe (Figure S2).

The frequency dependence of the ac susceptibility measured under applied dc fields of 500 Oe and 2000 Oe, is shown in Figure 3 and Figure S3 for **1** and **2**, respectively. Despite the application of these static fields, neither complex exhibited a distinct maximum in the out-of-phase susceptibility component, limiting the ability to perform a detailed analysis of the relaxation dynamics. However, the noticeable increase in χ'' for complex **1** under applied fields suggests an improvement in its slow relaxation behavior compared to complex **2**. Although no clear maxima were observed for complex **1**, a flattening of the χ'' as the temperature rises was evident. This absence of maxima is further confirmed by the Cole-Cole plots (Figure S4). We believe this behavior suggests a complex relaxation process, likely reflecting a broad distribution of relaxation times.

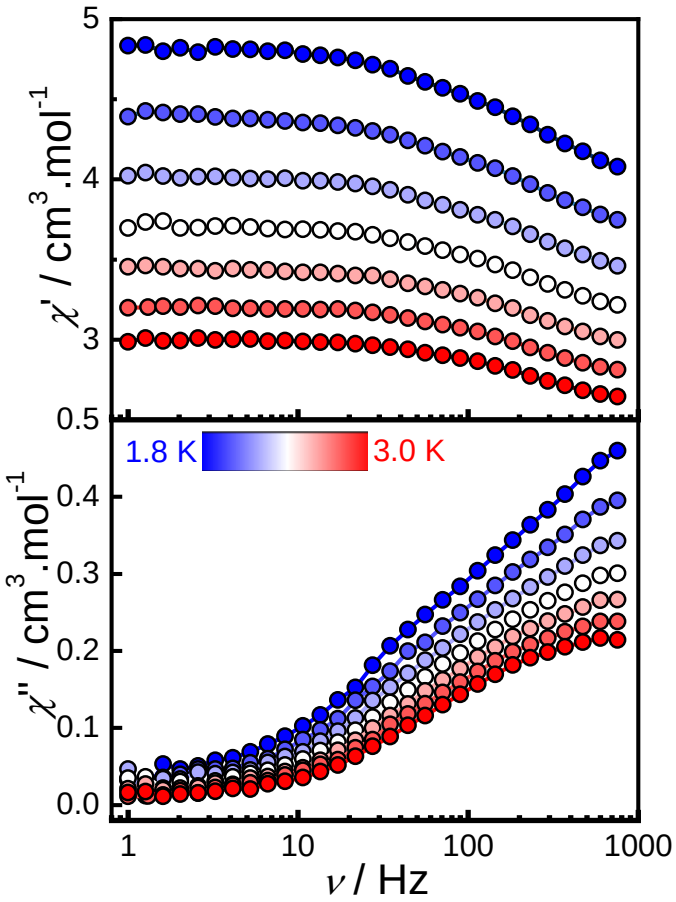

Figure 3. Frequency dependence of the in-phase (χ') and out-of phase (χ'') susceptibilities for **1** under a 500 Oe dc-field.

Theoretical Calculations. To gain a deeper understanding of the magnetic anisotropy in these tetranuclear systems, *ab initio* calculations were conducted at the CASSCF level using the ORCA package.[56] Individual fragments related the unique crystallographically Dy^{3+} ion were obtained by substituting one Dy^{3+} ion by diamagnetic Y^{3+} ions. For complex **2**, the Cu^{2+} ions were replaced with diamagnetic Zn^{2+} ions.

These calculations reveal substantial variations in the magnetic anisotropy between the Dy^{3+} sites in the two complexes. Although both Dy^{3+} sites exhibit similar total CF splitting energies of about 500 cm^{-1}, the Dy^{3+} ion in complex **1** displays greater axiality with a g_z value of 17.2122 to be compared with the value of g_z = 15.1358 for complex **2** (Table 2). The first excited KD state lies at a slightly higher energy (40 cm^{-1}) in complex **1** compared to complex **2** (29 cm^{-1}).

Despite these observed axiality trends, the analysis of the ground state KD suggests that neither complex is "highly axial." The KD ground states are notably mixed with $m_J = |\pm 15/2>$ contributions of 78 and 69 % for **1** and **2**, respectively (Tables S5-S6). These mixed ground states, along with the presence of substantial transverse components in the *g*-tensors (Table 2), suggests strong QTM, consistent with the observed magnetic behavior. Moreover, the transition probabilities computed from SINGLE_ANISO reveals that it is found twice greater for **2** (Figure 4), which aligns with the observed ac susceptibility behavior. To further validate this, the QTM relaxation rate, τ_{QTM}^{-1}, was estimated using a model established in the literature for Kramers ions under a zero dc-field:[63]

$$\tau_{QTM}^{-1} = \frac{\beta H_{ave}}{h} \times \frac{g_{xy}^2}{2(g_{xy+}^2 g_z^2)^{1/2}} \text{ with } g_{xy} = \sqrt{g_x^2 + g_y^2}$$

While this model involves some approximations, its validity has been confirmed in many dysprosium systems.[64-69] Considering an average internal magnetic field H_{ave} of 20 mT, the estimated zero-field QTM relaxation times, τ_{QTM}, are 1.45×10^{-8} s and 3.85×10^{-9} s for complexes **1** and **2**, respectively. These very short τ_{QTM} values explain the absence of zero-field slow relaxation of the magnetization in both complexes. In addition, the observed out-of-phase signal for complex **1** upon applying a dc field is consistent with its greater τ_{QTM} value.

The calculations further reveal that the anisotropic axes for both Dy^{3+} centers are primarily influenced by a Dy-O bond involving a phenoxide oxygen from the Dy_2O_2 core (Figure S5). This bond, in conjunction with an oxygen atom ligand, forms a near-linear O-Dy-O arrangement that defines the preferred magnetic orientation. However complex **2** exhibits a more pronounced deviation from this alignment, which most likely decrease the magnetic anisotropy.

This analysis at the Dy^{3+} single-ion level demonstrates how the substitution of Ni^{2+} with Cu^{2+} significantly influences the magnetic anisotropy of the Dy^{3+} centers by altering their coordination environments. Despite a more distorted square antiprism geometry indicated by SHAPE analysis, complex **1** achieves greater axiality.

Table 2: Energy of the lowest Kramers doublets (KD) and their associated *g* tensors on the individual Dy fragments for **1** and **2**.

1			**2**	
KD	**Energy (cm^{-1})**	***g* tensor**	**Energy (cm^{-1})**	***g* tensor**
1	0	$g_x = 0.7508$ $g_y = 2.8338$ $g_z = 17.2122$	0	$g_x = 1.0390$ $g_y = 5.3590$ $g_z = 15.1358$
2	40	$g_x = 0.6040$ $g_y = 2.3524$ $g_z = 14.6286$	29	$g_x = 1.7094$ $g_y = 2.8764$ $g_z = 12.9081$
3	94	$g_x = 1.4182$ $g_y = 4.1174$ $g_z = 12.7490$	94	$g_x = 1.9522$ $g_y = 3.8446$ $g_z = 13.1833$
4	177	$g_x = 3.2590$ $g_y = 5.9161$ $g_z = 8.9839$	177	$g_x = 9.0551$ $g_y = 6.3097$ $g_z = 3.1190$
5	292	$g_x = 0.6180$ $g_y = 1.9042$ $g_z = 12.6907$	291	$g_x = 0.7050$ $g_y = 2.3413$ $g_z = 12.8144$
6	434	$g_x = 0.5186$ $g_y = 1.014$ $g_z = 14.9416$	417	$g_x = 0.9870$ $g_y = 1.6990$ $g_z = 16.1215$
7	462	$g_x = 0.2255$ $g_y = 0.9863$ $g_z = 16.9530$	444	$g_x = 0.8788$ $g_y = 2.0120$ $g_z = 13.6530$
8	518	$g_x = 0.2486$ $g_y = 0.6729$ $g_z = 17.0756$	500	$g_x = 0.4757$ $g_y = 1.4866$ $g_z = 16.6899$

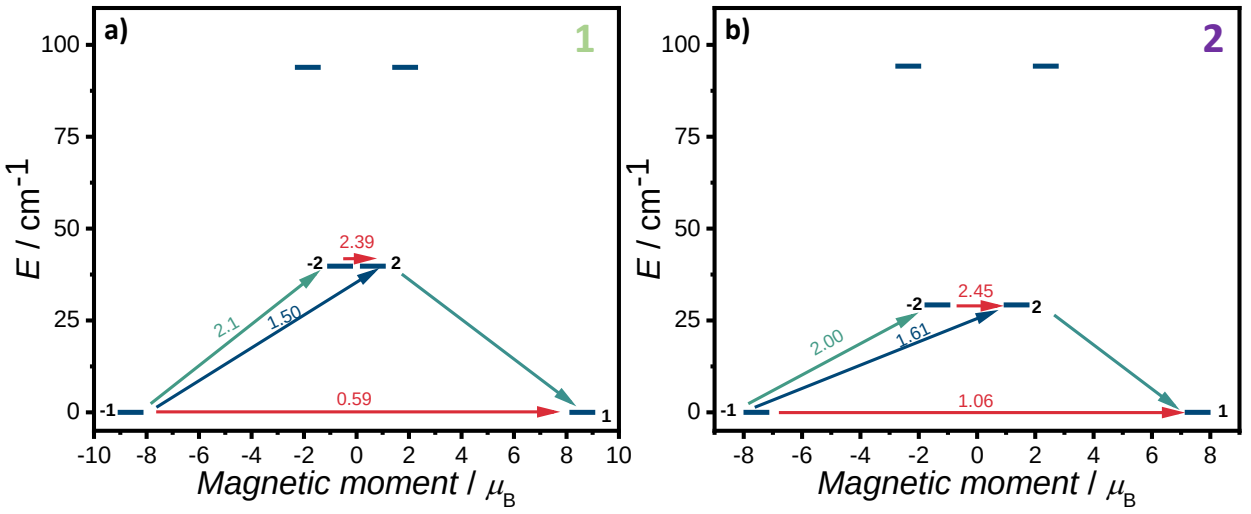

Figure 4. Energy diagram for low-lying KDs and transition magnetic moment matrix elements[70] (in μB) for the connected states for fragments **1** and **2**. For each KD (*n*), the corresponding states

(–*n*, *n*) are placed according to their magnetic moments. The horizontal arrows show the QTM transitions within each doublet, whereas the non-horizontal arrows are spin-phonon transition paths. Only the three first KDs are shown.

The non-axial nature of the Dy^{3+} ions, with g_z values of 17.2122 and 15.1358 for complexes **1** and **2**, respectively, precludes their treatment as Ising spins within the POLY_ANISO framework. While the POLY_ANISO package introduces an effective isotropic Heisenberg Hamiltonian parameterized by a single Lines exchange parameter, this model is exact only in the limiting cases of strongly axial doublets or isotropic spins on both sites.[71, 72] Consequently, the applicability of such treatment to our complexes is limited due to the non-axial nature of the Dy^{3+} ions.

Although ferromagnetic interactions are observed in complex **2**, they do not enhance the SMM behavior. These findings align with previous observations in a similar Cu_2 Dy_2 core bridged by carbonato ligands, where ferromagnetic interactions may lower the energy of the exchange-coupled states and QTM.[60] More generally, the ferromagnetic coupling between Cu^{2+} and Dy^{3+} ions may disrupt the Kramers doublet nature of the Dy^{3+} ions, a crucial factor in promoting slow relaxation of the magnetization.

Despite the modest observed SMM features, this study can be placed within the broader context of spin-state control of molecular complexes, which is typically focused on single-spin systems. For example, a recent study on a polynuclear Ni_5Dy SMM showed that a change in a coordination number change of a Ni^{2+} center can trigger a spin-state transition, altering the magnetic interactions and, in turn, the SMM properties. Our work offers a different perspective,

demonstrating how the modulation of the transition metal ion itself can be used to adjust magnetic interactions and SMM behavior without affecting the overall structure.

Conclusions

This work presents two novel heterometallic tetranuclear complexes, $[M_2\ Dy_2\ (Hheb)_2\ (heb)_4\ ]\cdot 4MeOH$ (M = Ni (**1**), Cu (**2**)), characterized by a rare zig-zag core topology driven by the rigid $Hheb^-$ /heb^{2-} ligands. Our investigation reveals a nuanced interplay between the incorporated 3d metal ions (Ni^{2+} and Cu^{2+}) and the magnetic properties of the complexes. While these systems exhibit signs of field-induced slow relaxation features, they do not allow for an in-depth analysis of the relaxation dynamics.

Nevertheless, we demonstrated that the choice of the 3d metal ion indirectly modulates the coordination environment and axiality of the Dy^{3+} ions, as confirmed by theoretical calculations. Specifically, Ni^{2+} ion in complex **1** promotes greater axiality of the Dy^{3+} ions, resulting in enhanced slow relaxation dynamics. Conversely, the introduction of Cu^{2+} in complex **2** decreases the magnetic anisotropy of the Dy^{3+} ion, with accompanying ferromagnetic interactions that do not favorably influence SMM behavior.

These findings can be contextualized within the broader framework of spin-state control in molecular systems, where tuning the local environment around metal ions plays a crucial role in regulating magnetic interactions and SMM properties. Our study highlights an alternative approach in which modulation of the transition metal ion itself offers a direct route to control magnetic interactions without altering the core structure. These insights open up possibilities for exploring other 3d metal ions and ligand frameworks to further optimize SMM performance.

ASSOCIATED COTENT

Supporting Information.

Additional crystallographic parameters, magnetic and theoretical data. The following files are available free of charge. Crystallographic data for **1-2** as CIF files (including structure factors) have been deposited at the Cambridge Crystallographic Data Centre as Supplementary Publication N° CCDC 2201892-2201895. Copies of the data can be obtained free of charge on application to CCDC, 12 Union Road, Cambridge CB2 1EZ, UK (fax: (+44) 1223-336-033; e-mail: deposit@ccdc.cam.ac.uk).

AUTHOR INFORMATION

Corresponding Author

*E-mail: jerome.long@umontpellier.fr
*E-mail: poheng@dragon.nchu.edu.tw

Author Contributions

The manuscript was written through contributions of all authors. All authors have given approval to the final version of the manuscript.

ACKNOWLEDGMENT

The authors thank the University of Montpellier, CNRS and PAC of ICGM. J. Long also acknowledges the support from the Institut Universitaire de France. We also gratefully acknowledge the financial support from National Chung Hsing University and the Ministry of Science and Technology, Taiwan MOST 112-2113-M-005-011 to P.-H. Lin.

REFERENCES

1. Luzon, J.; Sessoli, R., Lanthanides in molecular magnetism: so fascinating, so challenging. *Dalton Trans.* **2012,** *41* (44), 13556-13567.
2. Woodruff, D. N.; Winpenny, R. E. P.; Layfield, R. A., Lanthanide single-molecule magnets. *Chem. Rev.* **2013,** *113* (7), 5110-5148.
3. Troiani, F.; Affronte, M., Molecular spins for quantum information technologies. *Chem. Soc. Rev.* **2011,** *40* (6), 3119-3129.
4. Bogani, L.; Wernsdorfer, W., Molecular spintronics using single-molecule magnets. *Nat. Mater.* **2008,** *7* (3), 179-186.
5. Layfield, R. A.; Murugesu, M., *Lanthanides and Actinides in Molecular Magnetism*. Wiley: 2015.
6. Liu, J.-L.; Chen, Y.-C.; Tong, M.-L., Symmetry strategies for high performance lanthanide-based single-molecule magnets. *Chem. Soc. Rev.* **2018,** *47* (7), 2431-2453.
7. Layfield, R. A., Organometallic Single-Molecule Magnets. *Organometallics* **2014,** *33* (5), 1084-1099.
8. Goodwin, C. A. P.; Ortu, F.; Reta, D.; Chilton, N. F.; Mills, D. P., Molecular magnetic hysteresis at 60 kelvin in dysprosocenium. *Nature* **2017,** *548* (7668), 439-442.
9. Guo, F.-S.; Day, B. M.; Chen, Y.-C.; Tong, M.-L.; Mansikkamäki, A.; Layfield, R. A., Magnetic hysteresis up to 80 kelvin in a dysprosium metallocene single-molecule magnet. *Science* **2018,** *362* (6421), 1400-1403.
10. Randall McClain, K.; Gould, C. A.; Chakarawet, K.; Teat, S. J.; Groshens, T. J.; Long, J. R.; Harvey, B. G., High-temperature magnetic blocking and magneto-structural correlations in a series of dysprosium(iii) metallocenium single-molecule magnets. *Chem. Sci.* **2018,** *9* (45), 8492-8503.
11. Liu, J.; Chen, Y.-C.; Liu, J.-L.; Vieru, V.; Ungur, L.; Jia, J.-H.; Chibotaru, L. F.; Lan, Y.; Wernsdorfer, W.; Gao, S.; Chen, X.-M.; Tong, M.-L., A Stable Pentagonal Bipyramidal Dy(III) Single-Ion Magnet with a Record Magnetization Reversal Barrier over 1000 K. *J. Am. Chem. Soc.* **2016,** *138* (16), 5441-5450.
12. Ding, Y.-S.; Chilton, N. F.; Winpenny, R. E. P.; Zheng, Y.-Z., On Approaching the Limit of Molecular Magnetic Anisotropy: A Near-Perfect Pentagonal Bipyramidal Dysprosium(III) Single-Molecule Magnet. *Angew. Chem. Int. Ed.* **2016,** *55* (52), 16071-16074.
13. Ding, Y.-S.; Yu, K.-X.; Reta, D.; Ortu, F.; Winpenny, R. E. P.; Zheng, Y.-Z.; Chilton, N. F., Field- and temperature-dependent quantum tunnelling of the magnetisation in a large barrier single-molecule magnet. *Nat. Comm.* **2018,** *9* (1), 3134.
14. Ding, Y. S.; Han, T.; Zhai, Y. Q.; Reta, D.; Chilton, N. F.; Winpenny, R. E. P.; Zheng, Y. Z., A Study of Magnetic Relaxation in Dysprosium(III) Single-Molecule Magnets. *Chem. Eur. J.* **2020,** *26* (26), 5893-5902.
15. Yu, K.-X.; Kragskow, J. G.; Ding, Y.-S.; Zhai, Y.-Q.; Reta, D.; Chilton, N. F.; Zheng, Y.-Z., Enhancing Magnetic Hysteresis in Single-Molecule Magnets by Ligand Functionalization. *Chem* **2020,** *6* (7), 1777-1793.
16. Parmar, V.; Mills, D. P.; Winpenny, R., Mononuclear Dysprosium Alkoxide and Aryloxide Single-Molecule Magnets. *Chem. Eur. J.* **2021,** *27* (28), 7625-7645.
17. Long, J.; Tolpygin, A. O.; Mamontova, E.; Lyssenko, K. A.; Liu, D.; Albaqami, M. D.; Chibotaru, L. F.; Guari, Y.; Larionova, J.; Trifonov, A. A., An unusual mechanism of

building up of a high magnetization blocking barrier in an octahedral alkoxide Dy3+-based single-molecule magnet. *Inorg. Chem. Front.* **2021,** *8* (5), 1166-1174.
18. Ding, X.-L.; Zhai, Y.-Q.; Han, T.; Chen, W.-P.; Ding, Y.-S.; Zheng, Y.-Z., A Local D_{4h} Symmetric Dysprosium(III) Single-Molecule Magnet with an Energy Barrier Exceeding 2000 K**. *Chem. Eur. J.* **2021,** *27* (8), 2623-2627.
19. Xu, W. J.; Luo, Q. C.; Li, Z. H.; Zhai, Y. Q.; Zheng, Y. Z., Bis-Alkoxide Dysprosium(III) Crown Ether Complexes Exhibit Tunable Air Stability and Record Energy Barrier. *Adv. Science* **2024,** *11* (17), e2308548.
20. Giansiracusa, M. J.; Moreno-Pineda, E.; Hussain, R.; Marx, R.; Martínez Prada, M.; Neugebauer, P.; Al-Badran, S.; Collison, D.; Tuna, F.; van Slageren, J.; Carretta, S.; Guidi, T.; McInnes, E. J. L.; Winpenny, R. E. P.; Chilton, N. F., Measurement of Magnetic Exchange in Asymmetric Lanthanide Dimetallics: Toward a Transferable Theoretical Framework. *J. Am. Chem. Soc.* **2018,** *140* (7), 2504-2513.
21. Bajaj, N.; Mavragani, N.; Kitos, A. A.; Chartrand, D.; Maris, T.; Mansikkamäki, A.; Murugesu, M., Hard single-molecule magnet behavior and strong magnetic coupling in pyrazinyl radical-bridged lanthanide metallocenes. *Chem* **2024,** *10* (8), 2484-2499.
22. Blagg, R. J.; Ungur, L.; Tuna, F.; Speak, J.; Comar, P.; Collison, D.; Wernsdorfer, W.; McInnes, E. J. L.; Chibotaru, L. F.; Winpenny, R. E. P., Magnetic relaxation pathways in lanthanide single-molecule magnets. *Nat. Chem.* **2013,** *5* (8), 673-678.
23. Long, J.; Habib, F.; Lin, P.-H.; Korobkov, I.; Enright, G.; Ungur, L.; Wernsdorfer, W.; Chibotaru, L. F.; Murugesu, M., Single-molecule magnet behavior for an antiferromagnetically superexchange-coupled dinuclear dysprosium(III) complex. *J. Am. Chem. Soc.* **2011,** *133* (14), 5319-5328.
24. Katoh, K.; Asano, R.; Miura, A.; Horii, Y.; Morita, T.; Breedlove, B. K.; Yamashita, M., Effect of f-f interactions on quantum tunnelling of the magnetization: mono- and dinuclear Dy(iii) phthalocyaninato triple-decker single-molecule magnets with the same octacoordination environment. *Dalton Trans.* **2014,** *43* (21), 7716-7725.
25. Pineda, E. M.; Lan, Y.; Fuhr, O.; Wernsdorfer, W.; Ruben, M., Exchange-bias quantum tunnelling in a CO_2-based Dy_4-single molecule magnet. *Chem. Sci.* **2017,** *8* (2), 1178-1185.
26. Xiong, J.; Ding, H.-Y.; Meng, Y.-S.; Gao, C.; Zhang, X.-J.; Meng, Z.-S.; Zhang, Y.-Q.; Shi, W.; Wang, B.-W.; Gao, S., Hydroxide-bridged five-coordinate Dy^{III} single-molecule magnet exhibiting the record thermal relaxation barrier of magnetization among lanthanide-only dimers. *Chem. Sci.* **2017,** *8* (2), 1288-1294.
27. Bernbeck, M. G.; Orlova, A. P.; Hilgar, J. D.; Gembicky, M.; Ozerov, M.; Rinehart, J. D., Dipolar Coupling as a Mechanism for Fine Control of Magnetic States in ErCOT-Alkyl Molecular Magnets. *J. Am. Chem. Soc.* **2024,** *146* (11), 7243-7256.
28. Rinehart, J. D.; Fang, M.; Evans, W. J.; Long, J. R., Strong exchange and magnetic blocking in N_2^{3-}-radical-bridged lanthanide complexes. *Nat. Chem.* **2011,** *3* (7), 538-542.
29. Gould Colin, A.; McClain, K. R.; Reta, D.; Kragskow Jon, G. C.; Marchiori David, A.; Lachman, E.; Choi, E.-S.; Analytis James, G.; Britt, R. D.; Chilton Nicholas, F.; Harvey Benjamin, G.; Long Jeffrey, R., Ultrahard magnetism from mixed-valence dilanthanide complexes with metal-metal bonding. *Science* **2022,** *375* (6577), 198-202.
30. Kwon, H.; McClain, K. R.; Kragskow, J. G. C.; Staab, J. K.; Ozerov, M.; Meihaus, K. R.; Harvey, B. G.; Choi, E. S.; Chilton, N. F.; Long, J. R., Coercive Fields Exceeding 30 T in the Mixed-Valence Single-Molecule Magnet $(Cp^{iPr5})_2Ho_2I_3$. *J. Am. Chem. Soc.* **2024,** *146* (27), 18714-18721.

31. Qin, L.; Singleton, J.; Chen, W.-P.; Nojiri, H.; Engelhardt, L.; Winpenny, R. E. P.; Zheng, Y.-Z., Quantum Monte Carlo Simulations and High-Field Magnetization Studies of Antiferromagnetic Interactions in a Giant Hetero-Spin Ring. *Angew. Chem. Int. Ed.* **2017,** *56* (52), 16571-16574.
32. Zhou, G.-J.; Han, T.; Ding, Y.-S.; Chilton, N. F.; Zheng, Y.-Z., Metallacrowns as Templates for Diabolo-like {$LnCu_8$} Complexes with Nearly Perfect Square Antiprismatic Geometry. *Chem. Eur. J.* **2017,** *23* (62), 15617-15622.
33. Dey, A.; Bag, P.; Kalita, P.; Chandrasekhar, V., Heterometallic Cu^{II}–Ln^{III} complexes: Single molecule magnets and magnetic refrigerants. *Coord. Chem. Rev.* **2021,** *432*, 213707.
34. Ling, B.-K.; Zhai, Y.-Q.; Jin, P.-B.; Ding, H.-F.; Zhang, X.-F.; Lv, Y.; Fu, Z.; Deng, J.; Schulze, M.; Wernsdorfer, W.; Zheng, Y.-Z., Suppression of zero-field quantum tunneling of magnetization by a fluorido bridge for a "very hard" 3d-4f single-molecule magnet. *Matter* **2022,** *5* (10), 3485-3498.
35. Swain, A.; Sharma, T.; Rajaraman, G., Strategies to quench quantum tunneling of magnetization in lanthanide single molecule magnets. *Chem. Commun.* **2023,** *59* (22), 3206-3228.
36. Venkataramani, S.; Jana, U.; Dommaschk, M.; Sönnichsen, F. D.; Tuczek, F.; Herges, R., Magnetic Bistability of Molecules in Homogeneous Solution at Room Temperature. *Science* **2011,** *331* (6016), 445-448.
37. Nowak, R.; Prasetyanto, E. A.; De Cola, L.; Bojer, B.; Siegel, R.; Senker, J.; Rössler, E.; Weber, B., Proton-driven coordination-induced spin state switch (PD-CISSS) of iron(ii) complexes. *Chem. Commun.* **2017,** *53* (5), 971-974.
38. Ababei, R.; Pichon, C.; Roubeau, O.; Li, Y.-G.; Bréfuel, N.; Buisson, L.; Guionneau, P.; Mathonière, C.; Clérac, R., Rational Design of a Photomagnetic Chain: Bridging Single-Molecule Magnets with a Spin-Crossover Complex. *J. Am. Chem. Soc.* **2013,** *135* (39), 14840-14853.
39. Deng, W.; Wu, S.-G.; Ruan, Z.-Y.; Gong, Y.-P.; Du, S.-N.; Wang, H.-L.; Chen, Y.-C.; Zhang, W.-X.; Liu, J.-L.; Tong, M.-L., Spin-State Control in Dysprosium(III) Metallacrown Magnets via Thioacetal Modification. *Angew. Chem. Int. Ed.* **2024,** *63* (31), e202404271.
40. Habib, F.; Murugesu, M., Lessons learned from dinuclear lanthanide nano-magnets. *Chem. Soc. Rev.* **2013,** *42* (8), 3278-3288.
41. Cen, P.; Liu, X.; Zhang, Y.-Q.; Ferrando-Soria, J.; Xie, G.; Chen, S.; Pardo, E., Modulating magnetic dynamics through tailoring the terminal ligands in Dy_2 single-molecule magnets. *Dalton Trans.* **2020,** *49* (3), 808-816.
42. Bera, S. P.; Mondal, A.; Konar, S., Investigation of the role of terminal ligands in magnetic relaxation in a series of dinuclear dysprosium complexes. *Inorg. Chem. Front.* **2020,** *7* (18), 3352-3363.
43. Zhang , L.; Jung, J.; Zhang, P.; Guo, M.; Zhao, L.; Tang, J.; Le Guennic, B., Site-Resolved Two-Step Relaxation Process in an Asymmetric Dy_2 Single-Molecule Magnet. *Chem. Eur. J.* **2016,** *22* (4), 1392-1398.
44. Zhang, L.; Zhang, Y.-Q.; Zhang, P.; Zhao, L.; Guo, M.; Tang, J., Single-Molecule Magnet Behavior Enhanced by Synergic Effect of Single-Ion Anisotropy and Magnetic Interactions. *Inorg. Chem.* **2017,** *56* (14), 7882-7889.
45. Zhang, W.; Xu, S.-M.; Zhu, Z.-X.; Ru, J.; Zhang, Y.-Q.; Yao, M.-X., Strong intramolecular Dy^{III}–Dy^{III} magnetic couplings up to 15.00 cm−1 in phenoxyl-bridged dinuclear 4f complexes. *New. J. Chem.* **2020,** *44* (5), 2083-2090.

46. Yuan, Q.; Meng, Y.-S.; Zhang, Y.-Q.; Gao, C.; Liu, S.-S.; Wang, B.-W.; Gao, S., Synthesis and structures of fluoride-bridged dysprosium clusters: influence of fluoride ions on magnetic relaxation behaviors. *Inorg. Chem. Front.* **2022,** *9* (10), 2336-2342.
47. Kuppusamy, S. K.; Moreno-Pineda, E.; Nonat, A. M.; Heinrich, B.; Karmazin, L.; Charbonnière, L. J.; Ruben, M., Binuclear Lanthanide Complexes Based on 4-Picoline-N-oxide: From Sensitized Luminescence to Single-Molecule Magnet Characteristics. *Cryst. Growth Des.* **2023,** *23* (2), 1084-1094.
48. Nematirad, M.; Gee, W. J.; Langley, S. K.; Chilton, N. F.; Moubaraki, B.; Murray, K. S.; Batten, S. R., Single molecule magnetism in a μ-phenolato dinuclear lanthanide motif ligated by heptadentate Schiff base ligands. *Dalton Trans.* **2012,** *41* (44), 13711-13715.
49. Peng, Y.; Mereacre, V.; Baniodeh, A.; Lan, Y.; Schlageter, M.; Kostakis, G. E.; Powell, A. K., Effect of Ligand Field Tuning on the SMM Behavior for Three Related Alkoxide-Bridged Dysprosium Dimers. *Inorg. Chem.* **2016,** *55* (1), 68-74.
50. Wang, M.-H.; Tsai, M.-Y.; Su, Y.-C.; Chiu, S.-T.; Lin, P.-H.; Long, J., Zero-Field Single-Molecule Magnet Behavior in a Series of Dinuclear Dysprosium(III) Complexes Based on Benzothiazolyl-Based Ligands and β-Diketonates. *Cryst. Growth Des.* **2023,** *24* (1), 422-431.
51. Andruh, M.; Costes, J.-P.; Diaz, C.; Gao, S., 3d−4f Combined Chemistry: Synthetic Strategies and Magnetic Properties. *Inorg. Chem.* **2009,** *48* (8), 3342-3359.
52. Liu, K.; Shi, W.; Cheng, P., Toward heterometallic single-molecule magnets: Synthetic strategy, structures and properties of 3d–4f discrete complexes. *Coord. Chem. Rev.* **2015,** *289-290*, 74-122.
53. Wang, H.-S.; Zhang, K.; Song, Y.; Pan, Z.-Q., Recent advances in 3d-4f magnetic complexes with several types of non-carboxylate organic ligands. *Inorg. Chim. Acta* **2021,** *521*, 120318.
54. Wang, H.-L.; Zhu, Z.-H.; Peng, J.-M.; Zou, H.-H., Heterometallic 3d/4f-Metal Complexes: Structure and Magnetism. *J. Cluster Sci.* **2022,** *33* (4), 1299-1325.
55. Manne, R.; Miller, M.; Duthie, A.; Guedes da Silva, M. F. C.; Tshuva, E. Y.; Basu Baul, T. S., Cytotoxic homoleptic Ti(iv) compounds of ONO-type ligands: synthesis, structures and anti-cancer activity. *Dalton Trans.* **2019,** *48* (1), 304-314.
56. Neese, F., The ORCA program system. *WIREs Computational Molecular Science* **2012,** *2* (1), 73-78.
57. Neese, F., Software update: The ORCA program system-Version 5.0. *Wires Comput Mol Sci* **2022,** *12* (5), e1606.
58. Ungur, L.; Chibotaru, L. F. *SINGLE_ANISO Program*, 2006-2013.
59. Huang, X.-C.; Zhao, X.-H.; Shao, D.; Wang, X.-Y., Syntheses, structures, and magnetic properties of a family of end-on azido-bridged Cu^{II}–Ln^{III} complexes. *Dalton Trans.* **2017,** *46* (22), 7232-7241.
60. Maity, S.; Mondal, A.; Konar, S.; Ghosh, A., The role of 3d–4f exchange interaction in SMM behaviour and magnetic refrigeration of carbonato bridged $Cu^{II2}Ln^{III2}$ (Ln = Dy, Tb and Gd) complexes of an unsymmetrical N_2O_4 donor ligand. *Dalton Trans.* **2019,** *48* (40), 15170-15183.
61. Wu, H.; Li, M.; Zhang, S.; Ke, H.; Zhang, Y.; Zhuang, G.; Wang, W.; Wei, Q.; Xie, G.; Chen, S., Magnetic Interaction Affecting the Zero-Field Single-Molecule Magnet Behaviors in Isomorphic $\{Ni^{II2}Dy^{III2}\}$ and $\{Co^{II2}Dy^{III2}\}$ Tetranuclear Complexes. *Inorg. Chem.* **2017,** *56* (18), 11387-11397.

62. Casanova, D.; Llunell, M.; Alemany, P.; Alvarez, S., The Rich Stereochemistry of Eight-Vertex Polyhedra: A Continuous Shape Measures Study. *Chem. Eur. J.* **2005,** *11* (5), 1479-1494.
63. Yin, B.; Li, C.-C., A method to predict both the relaxation time of quantum tunneling of magnetization and the effective barrier of magnetic reversal for a Kramers single-ion magnet. *Phys. Chem. Chem. Phys.* **2020,** *22* (18), 9923-9933.
64. Jia, S.; Zhu, X.; Yin, B.; Dong, Y.; Sun, A.; Li, D.-f., Macrocyclic Hexagonal Bipyramidal Dy(III)-Based Single-Molecule Magnets with a D_{6h} Symmetry. *Cryst. Growth Des.* **2023,** *23* (9), 6967-6973.
65. Zhu, L.; Yin, B.; Ma, P.; Li, D., Tuning the Equatorial Crystal-Field in Mononuclear DyIII Complexes to Improve Single-Molecule Magnetic Properties. *Inorg. Chem.* **2020,** *59* (22), 16117-16121.
66. Zhu, Z.-H.; Wang, H.-F.; Yu, S.; Zou, H.-H.; Wang, H.-L.; Yin, B.; Liang, F.-P., Substitution Effects Regulate the Formation of Butterfly-Shaped Tetranuclear Dy(III) Cluster and Dy-Based Hydrogen-Bonded Helix Frameworks: Structure and Magnetic Properties. *Inorg. Chem.* **2020,** *59* (16), 11640-11650.
67. Zhang, S.; Tang, J.; Zhang, J.; Xu, F.; Chen, S.; Hu, D.; Yin, B.; Zhang, J., In Situ Ligand Formation in the Synthetic Processes from Mononuclear Dy(III) Compounds to Binuclear Dy(III) Compounds: Synthesis, Structure, Magnetic Behavior, and Theoretical Analysis. *Inorg. Chem.* **2021,** *60* (2), 816-830.
68. Mondal, A.; Konar, S., Effect of an axial coordination environment on quantum tunnelling of magnetization for dysprosium single-ion magnets with theoretical insight. *Dalton Trans.* **2022,** *51* (4), 1464-1473.
69. Shen, N.; Liang, J.; Qu, X.; Liu, S.; Zhu, L.; Zhang, S.; Chen, L.; Zhang, J.; Hu, D.; Yin, B., The influence of organic bases and substituted groups on coordination structures affording two mononuclear Dy(iii) single-molecule magnets (SMMs) and a novel Dy(iii)–K(i) compound with unusually coordinated fluorine atoms. *Cryst. Eng. Comm.* **2021,** *23* (22), 4013-4027.
70. Ungur, L.; Chibotaru, L. F., Strategies toward High-Temperature Lanthanide-Based Single-Molecule Magnets. *Inorg. Chem.* **2016,** *55* (20), 10043-10056.
71. Ungur, L.; Thewissen, M.; Costes, J.-P.; Wernsdorfer, W.; Chibotaru, L. F., Interplay of Strongly Anisotropic Metal Ions in Magnetic Blocking of Complexes. *Inorg. Chem.* **2013,** *52* (11), 6328-6337.
72. Xue, S.; Guo, Y.-N.; Ungur, L.; Tang, J.; Chibotaru, L. F., Tuning the Magnetic Interactions and Relaxation Dynamics of Dy2 Single-Molecule Magnets. *Chem. Eur. J.* **2015,** *21* (40), 14099-14106.

For Table of Contents Use Only

Fine-Tuning of Magnetic Anisotropy in Tetranuclear M_2Dy_2 Complexes with Zig-Zag Topology: The Impact of 3d Metal Selection

Guan-Lin Lu,[a] Shih-Ting Chiu,[a] Jérôme Long *[b,c] and Po-Heng Lin*[a]

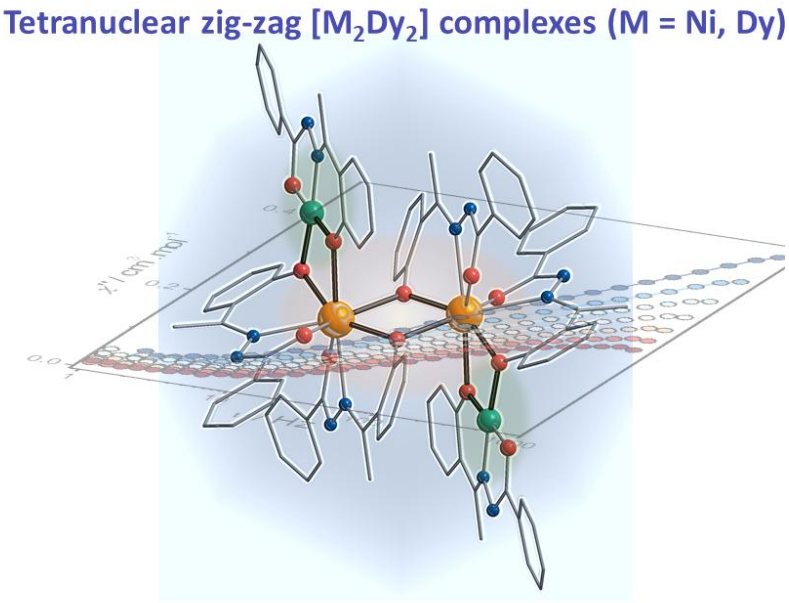

Two tetranuclear heterometallic $[M_2Dy_2]$ (M = Ni, Cu) complexes incorporating rigid $Hheb^{-}$ /heb^{2-} ligands demonstrate a rare zig-zag core topology. The choice of the 3d metal ion indirectly influences the Dy^{3+} ion's coordination environment and its axiality.